Fabrication of free-standing lithium niobate nanowaveguides down to 50 nm in width

Reinhard Geiss[1], Anton Sergeyev[2], Holger Hartung[1], Alexander S Solntsev[3], Andrey A Sukhorukov[3], Rachel Grange[2], Frank Schrempel[1], Ernst-Bernhard Kley[1], Andreas Tünnermann[1,4] and Thomas Pertsch[1]

[1] Institute of Applied Physics, Abbe Center of Photonics, Friedrich-Schiller-Universität Jena, Max-Wien-Platz 1, 07743 Jena, Germany
[2] Optical Nanomaterial Group, Institute for Quantum Electronics, Department of Physics, ETH Zurich, August-Piccard-Hof 1 HPT H10, 8093 Zurich, Switzerland
[3] Nonlinear Physics Center, Research School of Physics and Engineering, Australian National University, Canberra ACT 2601, Australia
[4] Fraunhofer Institute for Applied Optics and Precision Engineering, Albert-Einstein-Str. 7, 07745 Jena, Germany

E-mail: grange@phys.ethz.ch

Abstract

Nonlinear optical nanoscale waveguides are a compact and powerful platform for efficient wavelength conversion. The free-standing waveguide geometry opens a range of applications in microscopy for local delivery of light, where *in situ* wavelength conversion helps to overcome various wavelength-dependent issues, such as biological tissue damage. In this paper, we present an original patterning method for high-precision fabrication of free-standing nanoscale waveguides based on lithium niobate, a material with a strong second-order nonlinearity and a broad transparency window covering the visible and mid-infrared wavelength ranges. The fabrication process combines electron-beam lithography with ion-beam enhanced etching and produces nanowaveguides with lengths from 5 to 50 μm, widths from 50 to 1000 nm and heights from 50 to 500 nm, each with a precision of few nanometers. The fabricated nanowaveguides are tested in an optical characterization experiment showing efficient second-harmonic generation.

Keywords: nanoscale waveguide, lithium niobate, second-harmonic generation, ion-beam enhanced etching, electron-beam lithography

(Some figures may appear in colour only in the online journal)

1. Introduction

Photonic integration and miniaturization of optical devices opens a pathway to a broad range of applications including accurate sensing [1–3] or efficient signal processing [4, 5]. In order to reduce the footprint and to increase the performance of the respective devices by further miniaturization, the size of their basic building blocks has to be decreased down to the nanoscale. Nanowaveguides are suitable nanophotonic components potentially serving this purpose. They represent one of the essential building blocks for future photonic systems [6–8], since they can be used for efficient light transfer [9–11], optical switching [12] and lasing [13–15].

Despite the nanoscale size, nanowaveguides made of non-centrosymmetric materials still support nonlinear wave-mixing like sum-frequency [16, 17] and second-harmonic generations (SHGs) [16, 18–21]. Moreover, nanoscale waveguides can efficiently confine light in the form of guided modes, preventing diffractive light spreading and enhancing nonlinear interactions [22]. In particular, nanowaveguides can be used as light sources, which convert an input laser signal to a different wavelength through nonlinear wave mixing.

Additionally, detached nanowaveguides can be manipulated with an optical trap and can be even used for nanowire microscopy [23] or local light delivery to excite fluorescent material [23, 24].

Semiconductor nanowaveguides have been studied before due to their large nonlinear coefficient [25, 26] and relatively simple synthesis methods [27–29]. However, most semiconductor materials only work in a limited wavelength range since they strongly absorb visible light. In contrast, lithium niobate ($LiNbO_3$) possesses simultaneously a strong quadratic optical nonlinearity [25, 26] and a broad transparency window extending into the visible and infrared wavelength ranges. Moreover, the bio-compatibility of $LiNbO_3$ nanoparticles allows their application for biological studies [30].

Nanostructures made of $LiNbO_3$, especially nanowires, are usually produced by chemical synthesis that does not allow proper control of the dimensions and the crystal structure of the nanowires [31–34]. An alternative approach is the use of top-down fabrication methods. Focused-ion beam (FIB) milling, for example, is a commonly used maskless patterning technique with high precision. Nonetheless, it is slow and limited to small sample areas. Moreover, the FIB damages the crystal structure of the remaining substrate material which affects its optical properties [35, 36]. Other structuring technologies use lithographically patterned masks that are transferred into the $LiNbO_3$ substrate, for example by reactive-ion etching or ion-beam etching. These methods use low energy ions and cause less damage to the crystal structure. However, the shapes of the resulting patterns are very limited due to their strongly inclined sidewalls [37–41] that originate from the isotropic etching behavior. A more suitable pattern transfer technique is ion-beam enhanced etching (IBEE) [42], which was specifically developed for high aspect ratio nanostructures in $LiNbO_3$ [43, 44]. Basically, IBEE uses ion-beam irradiation to damage the crystal structure of the $LiNbO_3$. When the resulting defect density in the $LiNbO_3$ crystal exceeds a threshold value, the irradiated material can be removed by wet etching with high selectivity. IBEE can be used in combination with lithographically defined masks. The openings in the mask define the parts of the $LiNbO_3$ crystal to be locally damaged by the ion-beam irradiation. Typically, high-energy argon ions are used to broadly damage the $LiNbO_3$ from the surface down to a specific depth. If, in addition to the planar patterning, a configuration is required that comprises a membrane, helium-ion irradiations can be used to form a well-confined damaged layer. The position and height of this buried layer can be adjusted to connect to the regions damaged by preceding argon-ion irradiations. In this way, it is possible to fabricate detachable free-standing patterned membranes.

We have developed a patterning technique based on IBEE for the realization of suspended nanowaveguides that can be easily removed off the substrate. Furthermore, we present a comprehensive simulation of the fabrication process and outline its capabilities to precisely design and fabricate the cross-sectional shape of a nanowaveguide and to ensure its optical functionality, especially efficient SHG [22]. In the end, we demonstrate experimentally efficient generation and waveguiding of the second-harmonic in a nanowaveguide with a cross-section of $265 \times 287\,\mathrm{nm}^2$ and a length of 30.5 μm.

2. Fabrication process of the lithium niobate nanowaveguides

For the sample fabrication, a wafer of congruent x-cut $LiNbO_3$ with a thickness of 1 mm was used. To define the shape of the nanowaveguides, a mask was prepared on the top of the $LiNbO_3$ surface. Firstly, layers of fused silica (1000 nm), chromium (80 nm) and resist (300 nm, ZEP520A) were deposited onto the substrate (figure 1(a)). Secondly, the pattern layout was written into the resist by electron beam lithography (figure 1(b)). The pattern consisted of gratings with varied periods, filling factors and line lengths, where the grating ridges of the final structure represent the suspended nanowaveguides. The resist pattern was then transferred into the chromium and through the chromium into the silica by reactive ion etching. Afterwards, the remaining resist was removed by inductively coupled plasma reactive ion etching (figure 1(c)).

The obtained patterned layer was used to mask regions of the substrate surface during a series of argon-ion irradiations (figure 1(d)). The irradiation was performed at various energies: 600 keV with a fluence of $7.2 \cdot 10^{14}\,\mathrm{cm}^{-2}$ and 350, 150, 60 keV each with a fluence of $1.38 \cdot 10^{14}\,\mathrm{cm}^{-2}$. The resulting defect distribution in the crystal was designed to obtain a layer of homogeneously damaged material starting from the surface down to the designed depth of 500 nm [43].

After removing the fused silica and chromium layers by wet etching (figure 1(e)), the helium-ion irradiation with an energy of 285 keV and a fluence of $5 \cdot 10^{16}\,\mathrm{cm}^{-2}$ was performed at a temperature of 100 K (figure 1(f)). The cooling of the sample avoided an accumulation of helium bubbles that would otherwise result in blistering of the surface [45]. The helium-ion irradiation formed a buried damaged layer inside the crystal [46] with a thickness of 450 nm. The layer was positioned below the substrate surface and connected exactly with the damaged region created by the preceding argon-ion irradiations [43].

After the irradiations, the substrate was thermally annealed at 300 °C for 30 min to improve the selectivity of the subsequent etching [47]. The wet etching in diluted hydrofluoric acid (3.7%) at 40 °C for 20 min eventually removed the parts of the substrate that were sufficiently damaged by the ion-beam irradiation, whereas the non-irradiated regions mostly maintained their crystal structure and remained unetched. As a result, grids of free-standing nanowaveguides were obtained (figure 1(g)). Finally, the sample was thermally annealed for 1 h at 500 °C to completely restore the crystalline structure and the optical properties of the $LiNbO_3$ substrate. Scanning electron microscope (SEM) images of the resulting suspended grating structures are shown in figure 2(a). To allow for accessing a large range of shapes experimentally, we fabricated nanowaveguides with the widths of

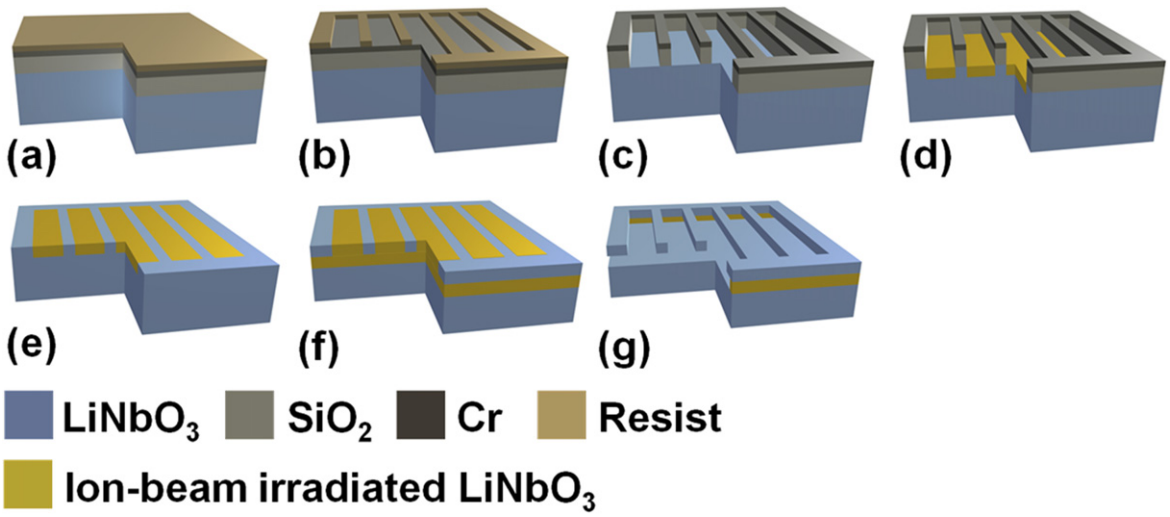

Figure 1. Schematic of the fabrication process: (a) lithium niobate substrate with layers of fused silica, chromium and resist; (b) electron-beam lithography of grids composed from nanowaveguides; (c) dry etching of chromium and fused silica; (d) argon-ion irradiation; (e) mask removal; (f) helium-ion irradiation; (g) wet etching.

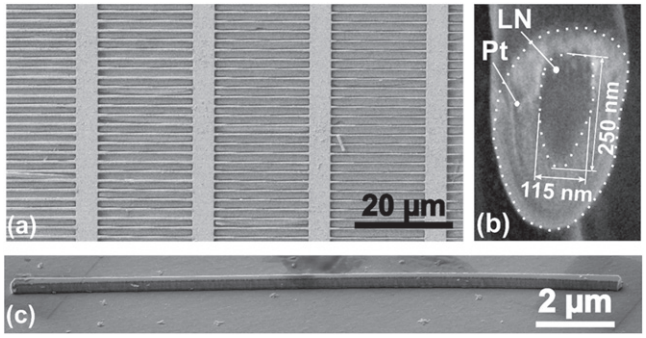

Figure 2. (a) SEM image of 20 μm long self-suspended lithium niobate (LN) nanowaveguides with different widths after the wet etching; (b) cross-section image of a nanowaveguide prepared by focused ion-beam milling. To preserve the edges during the milling a layer of platinum (Pt) was deposited around the waveguide; (c) SEM image of a typical nanowaveguide deposited on a glass substrate.

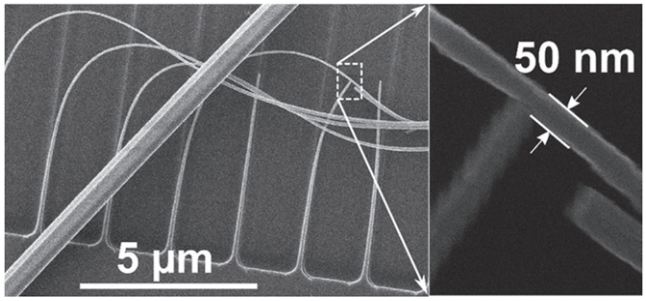

Figure 3. Helium ion microscope image of the smallest fabricated nanoscale waveguide with 50 nm width and 40 μm total length.

50–1000 nm, heights of 50–500 nm and lengths of 5–50 μm (figures 2 and 3). The irradiation conditions were chosen to result in perpendicular sidewalls and, hence, rectangular waveguide cross-sections. However, the final structures with widths below 200 nm exhibited a different shape as it is shown in a figure of a 115 nm wide nanowaveguide (figure 2(b)). Instead of being rectangular, the cross-sectional area is reduced in width at the bottom. Also, the height of the waveguide is significantly smaller than the 500 nm expected for the given helium-ion irradiation conditions. Further inspection of the sample revealed that the heights for nanowaveguides with widths below 200 nm were always smaller than the expected 500 nm. To understand this behavior and the limitations imposed by the fabrication, we simulated the ion-beam irradiation and the subsequent etching to compute the final shape of the waveguides.

3. Simulation of the nanowaveguide fabrication

The simulation of the ion-beam irradiation is based on SRIM (stopping and range of ions in matter) calculations [48], which computes the relative defect concentration in the $LiNbO_3$ crystal. In our simulation, we took into account the experimental ion irradiation conditions and material parameters of the $LiNbO_3$ substrate and of the lithographically patterned mask. For the subsequent etching simulation, we used the dependence of the etch rate on the defect concentration that was obtained experimentally [42]. Since waveguides are invariant in propagation direction, we performed our simulations only for two-dimensional cross-sections of the waveguides. For all of the following simulations, we keep the exact ion irradiation conditions that were used for the fabrication and vary the widths of the irradiation masks.

At first, we study irradiations that are performed only with argon ions to elucidate their influence on the shape of the nanowaveguides with widths below 200 nm. Figures 4(a)–(c) show the calculated defect distribution in a $LiNbO_3$ crystal created by the argon-ion irradiations for mask widths of 120 nm, 80 nm and 60 nm, respectively. The masks protect the underlying $LiNbO_3$ from the ion irradiation by stopping the ions. The unmasked areas allow the ions to penetrate and damage the $LiNbO_3$. Because of scattering, the defect

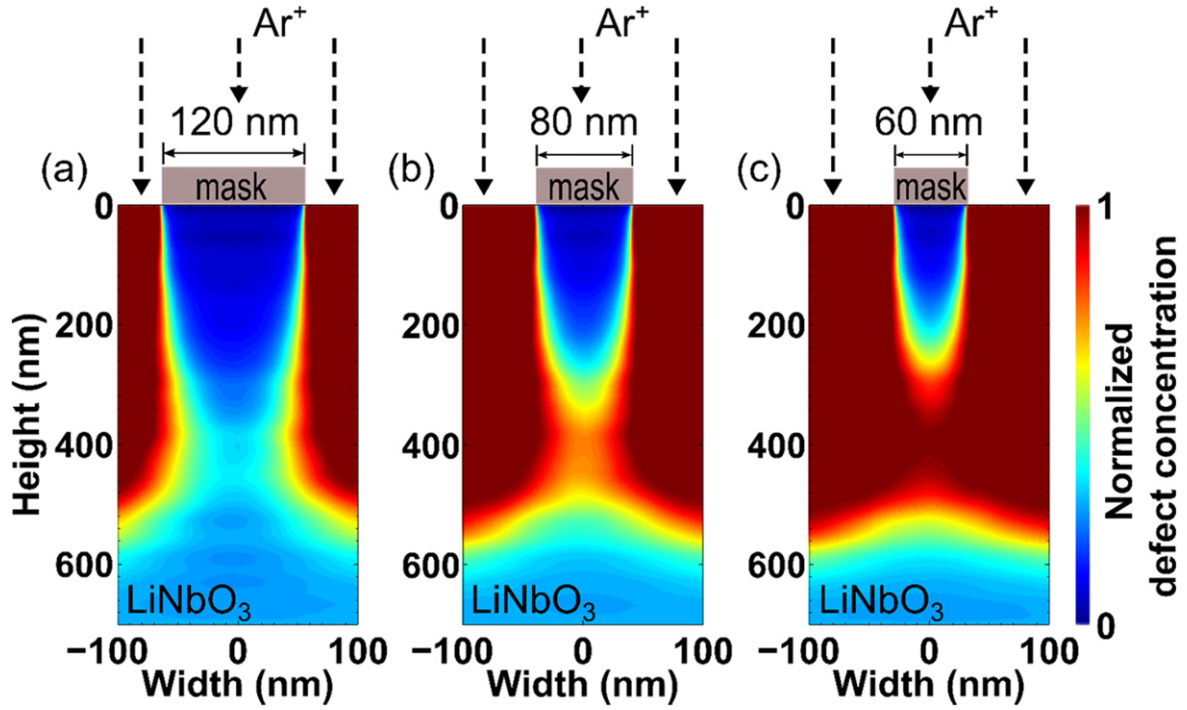

Figure 4. Spatial distribution of the normalized defect concentration induced by the argon-ion irradiations at mask widths of 120, 80, 60 nm.

distribution spreads along the ion beam leading to an exposure of regions that are situated underneath the mask. This effect is shown in figures 4(a)–(c), where the defect distribution reaches almost perpendicularly down from the surface and broadens at a certain penetration depth. For a mask width of 120 nm (figure 4(a)), the defected regions adjacent to the mask do not overlap. A partial overlap is obtained for a mask width of 80 nm (figure 4(b)) and a complete overlap for 60 nm (figure 4(c)). In the case of a complete overlap, the accumulated defect concentration is large enough to enable wet etching. The result is a narrow nanowaveguide with a height that is exclusively determined by the position and width of the defect distribution induced by the argon-ion irradiation.

In the next step, the complete fabrication process including the helium-ion irradiations is considered. The results are summarized in figure 5. The inset shows the computed shapes of the waveguide cross-sections that were obtained for different mask widths ranging from 50 nm to 1 μm. Furthermore, the aspect ratio (height/width) of the final nanowaveguide is plotted as a function of the mask widths in figure 5. As the plot shows, the highest aspect ratio of 3.6 was obtained at a width of 50 nm, and it decreases as the mask width increases. Moreover, the curve shows two different decaying behaviors (red dashed and green dotted lines) that switch at a width of 200 nm. This sudden change can be explained by the fact that the height reaches 500 nm, which is the maximum value pre-defined by the helium-ion irradiation. Thus, at widths above 200 nm, the height is exclusively determined by the helium-ion irradiation and does not change for increasing widths (green dotted line). In turn, at widths below 200 nm, the shape and, especially, the height of the

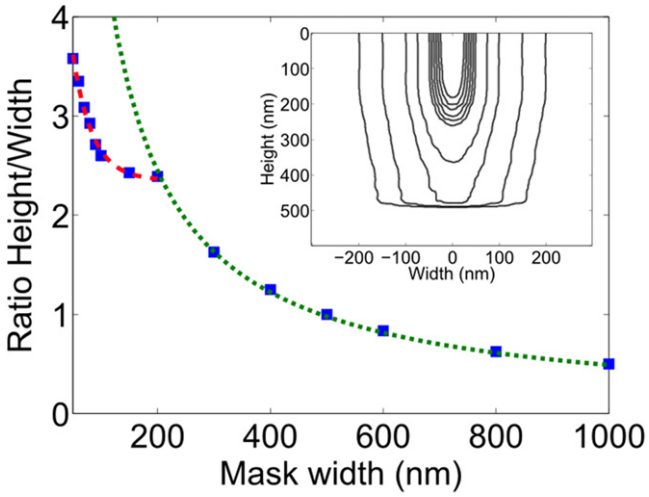

Figure 5. Computed dependence of the height/width ratio on the mask width. For widths below 200 nm, the shape and, especially, the height of the nanowaveguides are predominantly defined by the argon-ion irradiation (red dashed line). For widths above 200 nm, the height is defined by the helium-ion irradiation and, therefore, remains constant for increasing widths (green dotted line). The aspect ratio values (blue squares) are taken from the calculated cross-sectional areas (see inset) and fitted by two $1/x$ functions (red dashed and green dotted lines) to guide the eye. Inset: simulated cross-sectional areas of nanowaveguides with different mask widths.

nanowaveguides are mostly affected by the argon-ion irradiation (red dashed line). The presented theoretical findings agree very well with the fabricated structures. The cross-section of the nanowaveguide presented in figure 2(b), for example, shows good agreement with the calculated profile.

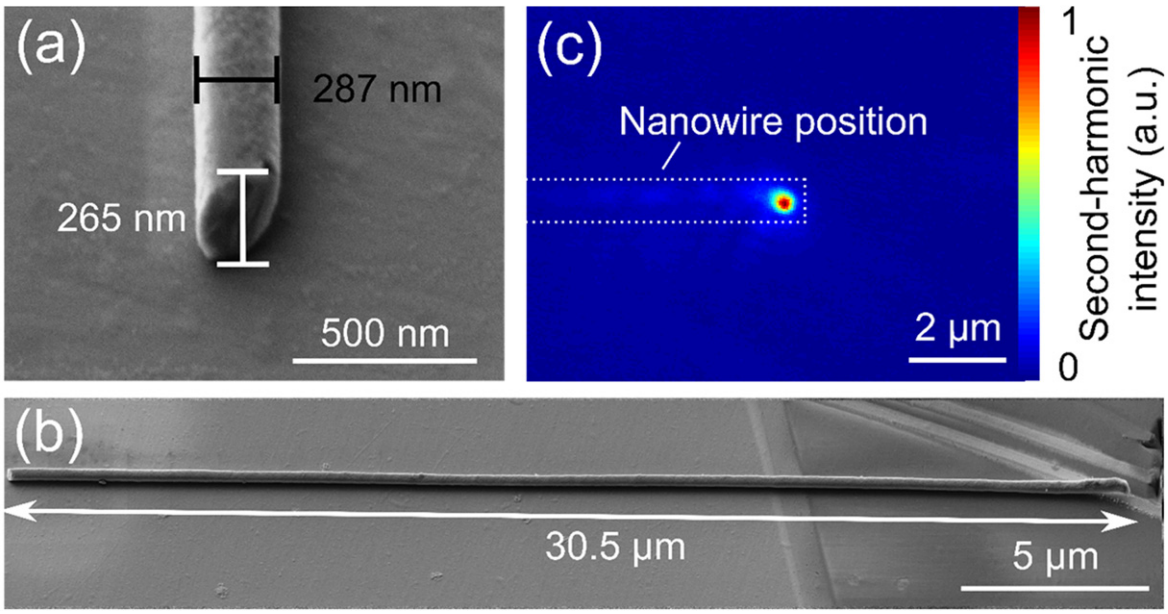

Figure 6. (a)–(b) SEM images of a nanowaveguide cross-section and of the nanowaveguide placed on another substrate. (c) Image of the guided second-harmonic signal. The dotted line indicates the nanowire position.

Using the simulation tool in combination with the presented fabrication scheme, precise control of the waveguide dimensions and shapes opens a possibility for the realization of optimal structures for nonlinear optical applications, such as SHG.

4. Optical testing of the nanowaveguides

In order to perform optical testing of a single nanowaveguide, we detached the nanowaveguides off the wafer by immersing the sample in ethanol and sonicating it for 7 s. A droplet of the obtained nanowaveguides–ethanol solution was then dried onto a silica substrate. The substrate was preliminarily coated with a conductive transparent indium tin oxide film to allow further inspection or manipulation with an SEM, FIB and optical microscopy.

Previously, we have demonstrated that nanowaveguides with dimensions of a few hundreds of nanometers are well suited for efficient modal phase-matching of the SHG [49]. Therefore, the majority of the presented nanowaveguides have been fabricated having dimensions in this range. On the other hand, the smallest waveguides presented in this work are intended to demonstrate that the fabrication of nanoscale high-aspect ratio structures with the widths down to 50 nm and micrometer lengths is feasible. The optical functionality of these small structures, including waveguiding and nonlinear optical properties, can be expected to be comparable to similar and smaller $LiNbO_3$ structures that are produced by chemical synthesis [32]. Detrimental effects originating from the IBEE patterning and potentially affecting the crystal structure and the optical properties of the small waveguides were fully removed in the final thermal annealing step [47].

The nanowaveguide with the smallest cross-section that was transferred onto another substrate using this method had dimensions of $265 \times 287\,nm^2$ and a length of 30.5 μm (figures 6(a) and (b)). The nonlinear optical characterization was carried out with a setup that has been used previously for similarly fabricated waveguides of larger size [24, 49]. The nanowaveguide presented here showed clear evidence of the SHG. In figure 6(c), we show an image of the guided second harmonic observed at the output facet of the waveguide. This guided second-harmonic signal was obtained when we focused the pump laser with a beam spot diameter of 5 μm onto the opposite nanowire facet. The pump laser had 760 nm wavelength, 283 fs pulse duration, 80 MHz repetition rate and an average power of 68 mW. The power of the guided second-harmonic signal was 62.7 fW which could be significantly optimized by phase-matching the interacting guided modes and by modifying the nanowaveguide facets for improving light coupling.

5. Conclusion

The fabricated nanoscale optical waveguides show a lot of promise due to their high nonlinearity, strong field confinement and potential for modal phase-matching of various frequency-conversion processes. The respective waveguides were successfully fabricated in $LiNbO_3$ using ion-beam enhanced etching in combination with electron beam lithography. The waveguides have lengths ranging from 5 to 50 μm and widths from 50 to 1000 nm. The heights of the nanowaveguides strongly depend on their widths and vary from 50 to 500 nm. A comprehensive simulation of the ion-beam irradiation process and the subsequent etching was performed to interpret the experimental findings. The final

waveguide shapes showed good agreement with the simulation results, therefore enabling the design of novel structures and geometries. The precise engineering of waveguide cross-sectional areas, to realize e.g. geometry-mediated modal phase-matching, becomes possible through the presented approach. In contrast to other lithography-based patterning schemes of $LiNbO_3$, this approach allows one to design through the simulation tool and fabricate the sidewall shape and steep edges of the nanowaveguides. For comparison, the dry etching method results in strongly inclined sidewalls that prohibit any high aspect ratio patterns [37–41]. It is further unique to the presented approach that the resulting nanowaveguide structures are free-standing and can be easily detached from the substrate. Eventually, the fabrication scheme was used to produce $LiNbO_3$ nanowaveguides that have been successfully tested optically and clearly showed efficient SHG [24]. In terms of size, free-standing geometry, and due to the sufficiently large frequency conversion efficiency, these waveguides can be understood as counterparts to chemically synthesized nanowires [34, 50, 51]. Through their well-defined sizes and shapes, these nanowaveguides allow further experimental developments harnessing the rich physics of nonlinear optics on the nanoscale for a variety of applications.

Acknowledgments

We acknowledge support from the Australian Research Council (Future Fellowship FT100100160 and Discovery Project DP130100135), from the German Federal Ministry of Education and Research (PhoNa), from the German Research Foundation (PE 1524/5-2 and KL 1199/2-2), and the German Academic Exchange Service (56265492).

References

[1] Martinez Vazquez R, Osellame R, Cretich M, Chiari M, Dongre C, Hoekstra H J W M, Pollnau M, van den Vlekkert H, Ramponi R and Cerullo G 2009 Optical sensing in microfluidic lab-on-a-chip by femtosecond-laser-written waveguides *Anal. Bioanal. Chem.* **393** 1209–16
[2] Crespi A *et al* 2010 Three-dimensional Mach–Zehnder interferometer in a microfluidic chip for spatially-resolved label-free detection *Lab Chip* **10** 1167–73
[3] Schult K, Katerkamp A, Trau D, Grawe F, Cammann K and Meusel M 1999 Disposable optical sensor chip for medical diagnostics: new ways in bioanalysis *Anal. Chem.* **71** 5430–5
[4] Almeida V R and Lipson M 2004 Optical bistability on a silicon chip *Opt. Lett.* **29** 2387–9
[5] Vlasov Y, Green W M J and Xia F 2008 High-throughput silicon nanophotonic wavelength-insensitive switch for on-chip optical networks *Nat. Photonics* **2** 242–6
[6] Barrelet C J, Greytak A B and Lieber C M 2004 Nanowire photonic circuit elements *Nano Lett.* **4** 1981–5
[7] Pauzauskie P J and Yang P 2006 Nanowire photonics *Mater. Today* **9** 36–45
[8] Yan R, Gargas D and Yang P 2009 Nanowire photonics *Nat. Photonics* **3** 569–76
[9] Voss T, Svacha G T, Mazur E, Müller S, Ronning C, Konjhodzic D and Marlow F 2007 High-order waveguide modes in ZnO nanowires *Nano Lett.* **7** 3675–80
[10] Yan R, Park J-H, Choi Y, Heo C-J, Yang S-M, Lee L P and Yang P 2012 Nanowire-based single-cell endoscopy *Nat. Nanotechnol.* **7** 191–6
[11] Palima D, Bañas A R, Vizsnyiczai G, Kelemen L, Ormos P and Glückstad J 2012 Wave-guided optical waveguides *Opt. Express* **20** 2004–14
[12] Piccione B, Cho C-H, van Vugt L K and Agarwal R 2012 All-optical active switching in individual semiconductor nanowires *Nat. Nanotechnol.* **7** 640–5
[13] Röder R, Wille M, Geburt S, Rensberg J, Zhang M, Lu J G, Capasso F, Buschlinger R, Peschel U and Ronning C 2013 Continuous wave nanowire lasing *Nano Lett.* **13** 3602–6
[14] Sidiropoulos T P H, Röder R, Geburt S, Hess O, Maier S A, Ronning C and Oulton R F 2014 Ultrafast plasmonic nanowire lasers near the surface plasmon frequency *Nat. Phys.* **10** 870–6
[15] Zhang C, Zou C-L, Yan Y, Hao R, Sun F-W, Han Z-F, Zhao Y S and Yao J 2011 Two-photon pumped lasing in single-crystal organic nanowire exciton polariton resonators *J. Am. Chem. Soc.* **133** 7276–9
[16] Barrelet C J, Ee H-S, Kwon S-H and Park H-G 2011 Nonlinear mixing in nanowire subwavelength waveguides *Nano Lett.* **11** 3022–5
[17] Zhang X, He H, Fan J, Gu C, Yan X, Hu M, Zhang X, Ren X and Wang C 2013 Sum frequency generation in pure zinc-blende GaAs nanowires *Opt. Express* **21** 28432
[18] Grange R *et al* 2012 Far-field imaging for direct visualization of light interferences in GaAs nanowires *Nano Lett.* **12** 5412–7
[19] Pernice W H P, Xiong C, Schuck C and Tang H X 2012 Second harmonic generation in phase matched aluminum nitride waveguides and micro-ring resonators *Appl. Phys. Lett.* **100** 223501
[20] Sanatinia R, Anand S and Swillo M 2014 Modal engineering of second-harmonic generation in single GaP nanopillars *Nano Lett.* **14** 5376–81
[21] Casadei A *et al* 2014 Photonic−plasmonic coupling of GaAs single nanowires to optical nanoantennas *Nano Lett.* **14** 2271–8
[22] Solntsev A S, Sukhorukov A A, Neshev D N, Iliew R, Geiss R, Pertsch T and Kivshar Y S 2011 Cascaded third harmonic generation in lithium niobate nanowaveguides *Appl. Phys. Lett.* **98** 231110
[23] Nakayama Y, Pauzauskie P J, Radenovic A, Onorato R M, Saykally R J, Liphardt J and Yang P 2007 Tunable nanowire nonlinear optical probe *Nature* **447** 1098–102
[24] Sergeyev A, Geiss R, Solntsev A S, Steinbrück A, Schrempel F, Kley E-B, Pertsch T and Grange R 2013 Second-harmonic generation in lithium niobate nanowires for local fluorescence excitation *Opt. Express* **21** 19012
[25] Boyd R W 2008 *Nonlinear Optics* (New York: Academic)
[26] Shoji I, Kondo T, Kitamoto A, Shirane M and Ito R 1997 Absolute scale of second-order nonlinear-optical coefficients *J. Opt. Soc. Am.* B **14** 17–9
[27] Wagner R S and Ellis W C 1964 Vapor–liquid–solid mechanism of single crystal growth *Appl. Phys. Lett.* **4** 89
[28] Moewe M, Chuang L C, Crankshaw S, Chase C and Chang-Hasnain C 2008 Atomically sharp catalyst-free wurtzite GaAs/AlGaAs nanoneedles grown on silicon *Appl. Phys. Lett.* **93** 023116
[29] Gudiksen M S and Lieber C M 2000 Diameter-selective synthesis of semiconductor nanowires *J. Am. Chem. Soc.* **122** 8801–2
[30] Staedler D *et al* 2012 Harmonic nanocrystals for biolabeling: a survey of optical properties and biocompatibility *ACS Nano* **6** 2542–9

[31] Grange R, Choi J-W, Hsieh C-L, Pu Y, Magrez A, Smajda R, Forro L and Psaltis D 2009 Lithium niobate nanowires synthesis, optical properties, and manipulation *Appl. Phys. Lett.* **95** 143105

[32] Dutto F, Raillon C, Schenk K and Radenovic A 2011 Nonlinear optical response in single alkaline niobate nanowires *Nano Lett.* **11** 2517–21

[33] He H, Zhang X, Yan X, Huang L and Gu C 2013 Broadband second harmonic generation in GaAs nanowires by femtosecond laser sources Broadband second harmonic generation in GaAs nanowires by femtosecond laser sources *Appl. Phys. Lett.* **103** 143110–4

[34] Santulli A C, Zhou H, Berweger S, Raschke M B, Sutter E and Wong S S 2010 Synthesis of single-crystalline one-dimensional $LiNbO_3$ nanowires *Cryst. Eng. Commun.* **12** 2675

[35] Draganski M A, Finkman E, Gibson B C, Fairchild B A, Ganesan K, Nabatova-Gabain N, Tomljenovic-Hanic S, Greentree A D and Prawer S 2013 The effect of gallium implantation on the optical properties of diamond *Diam. Relat. Mater.* **35** 47–52

[36] Geiss R, Diziain S, Steinert M, Schrempel F, Kley E-B, Tünnermann A and Pertsch T 2014 Photonic crystals in lithium niobate by combining focused ion beam writing and ion-beam enhanced etching *Phys. Status Solidi* **211** 2421–5

[37] Hu H, Ricken R and Sohler W 2009 Lithium niobate photonic wires *Opt. Express* **17** 24261–8

[38] Hines D S and Williams K E 2002 Patterning of wave guides in $LiNbO_3$ using ion beam etching and reactive ion beam etching *J. Vac. Sci. Technol.* A **20** 1072

[39] Mattiussi G, Lahoud N, Charbonneau R and Berini P 2007 Fabrication of long-range surface plasmon–polariton waveguides in lithium niobate on silicon *J. Vac. Sci. Technol.* A **25** 692

[40] Yang W S, Lee H-Y, Kim W K and Yoon D H 2005 Asymmetry ridge structure fabrication and reactive ion etching of $LiNbO_3$ *Opt. Mater.* **27** 1642–6

[41] Ulliac G, Courjal N, Chong H M H and Rue R M D L 2008 Batch process for the fabrication of $LiNbO_3$ photonic crystals using proton exchange followed by CHF_3 reactive ion etching *Opt. Mater.* **31** 196–200

[42] Schrempel F, Gischkat T, Hartung H, Kley E-B and Wesch W 2006 Ion beam enhanced etching of $LiNbO_3$ *Nucl. Instrum. Methods Phys. Res. Sect.* B **250** 164–8

[43] Hartung H, Kley E-B, Gischkat T, Schrempel F, Wesch W and Tünnermann A 2010 Ultra thin high index contrast photonic crystal slabs in lithium niobate *Opt. Mater.* **33** 19–21

[44] Geiss R, Saravi S, Sergeyev A, Diziain S, Setzpfandt F, Schrempel F, Grange R, Kley E B, Tünnermann A and Pertsch T 2015 Fabrication of nanoscale lithium niobate waveguides for second-harmonic generation *Opt. Lett.* **40** 2715–8

[45] Roth R M *et al* 2006 Compositional and structural changes in $LiNbO_3$ following deep He+ ion implantation for film exfoliation *Appl. Phys. Lett.* **89** 112906–1129063

[46] Schrempel F, Gischkat T, Hartung H, Höche T, Kley E-B, Tünnermann A and Wesch W 2009 Ultrathin membranes in x-cut lithium niobate *Opt. Lett.* **34** 1426

[47] Gischkat T, Schrempel F, Höche T and Wesch W 2009 Annealing behavior of lithium niobate irradiated with He-ions at 100 K *Nucl. Instrum. Methods Phys. Res.* B **267** 1492–5

[48] Ziegler J F, Ziegler M D and Biersack J P 2010 SRIM—the stopping and range of ions in matter (2010) *Nucl. Instrum. Methods Phys. Res.* B **268** 1818–23

[49] Sergeyev A, Geiss R, Solntsev A S, Sukhorukov A A, Schrempel F, Pertsch T and Grange R 2015 Enhancing guided second-harmonic light in lithium niobate nanowires *ACS Photonics* **2** 687–91

[50] Grange R, Dutto F and Radenovic A 2011 Niobates nanowires: synthesis, characterization and applications *Nanowires—Implementations and Applications* ed D A Hashim (Rijeka: InTech)

[51] Huang J, Chen Z, Zhang Z, Zhu C, He H, Ye Z, Qu G and Tong L 2011 Synthesis and waveguiding of single-crystalline $LiNbO_3$ nanorods *Appl. Phys. Lett.* **98** 093102